

Improving Sample Quality of Diffusion Models Using Self-Attention Guidance

Susung Hong, Gyuseong Lee, Wooseok Jang, Seungryong Kim

Korea University, Seoul, Korea



Figure 1: **Qualitative comparisons between guided and unguided samples by our method.** The top row is unguided samples from the original ADM (Dhariwal and Nichol 2021), and the bottom row is guided samples by our method. For the latter, the guidance is applied to the last one-third of the reverse process.

Abstract

Following generative adversarial networks (GANs), a *de facto* standard model for image generation, denoising diffusion models (DDMs) have been actively researched and attracted strong attention due to their capability to generate images with high quality and diversity. However, the way the internal self-attention mechanism works inside the UNet of DDMs is under-explored. To unveil them, in this paper, we first investigate the self-attention operations within the black-boxed diffusion models and build hypotheses. Next, we verify the hypotheses about the self-attention map by conducting frequency analysis and testing the relationships with the generated objects. In consequence, we find out that the attention map is closely related to the quality of generated images. On the other hand, diffusion guidance methods based on additional information such as labels are proposed to improve the quality of generated images. Inspired by these methods, we present label-free guidance based on the intermediate self-attention map that can guide existing pretrained diffusion models to generate images with higher fidelity. In addition to the enhanced sample quality when used alone, we show that the results are further improved by combining our method with classifier guidance on ImageNet 128×128 .

Introduction

Generative adversarial networks (GANs) (Goodfellow et al. 2014) have been a *de facto* model for the task of image generation. Recently, following GANs, denoising diffusion models (DDMs) (Ho, Jain, and Abbeel 2020) have been actively researched and attracted much attention for their remarkable capacity to generate images with the quality and diversity. In addition, DDMs have shown that they do not suffer from training instability and that they have superior scalability compared to GANs (Goodfellow et al. 2014).

Diffusion models have also engaged the self-attention mechanism (Vaswani et al. 2017). Denoising Diffusion Probabilistic Model (DDPM) (Ho, Jain, and Abbeel 2020) based implementations use the UNet structure (Ronneberger, Fischer, and Brox 2015) with self-attention (Vaswani et al. 2017) at a single resolution. ADM (Dhariwal and Nichol 2021) improved them by inserting self-attention layers to multiple resolutions.

There are chances to obtain intuitions by investigating the self-attention mechanism of these models. DINO (Caron et al. 2021) showed that the self-attention maps of the self-supervised transformers have an object-oriented property, and are effective for the object-oriented tasks such as semantic segmentation and video object segmentation. Specifically, several works (Van Gansbeke, Vandenhende, and Van Gool 2022; Zadaianchuk et al. 2022) use the attention

Project page is available at:
<https://ku-cvlab.github.io/Self-Attention-Guidance/>

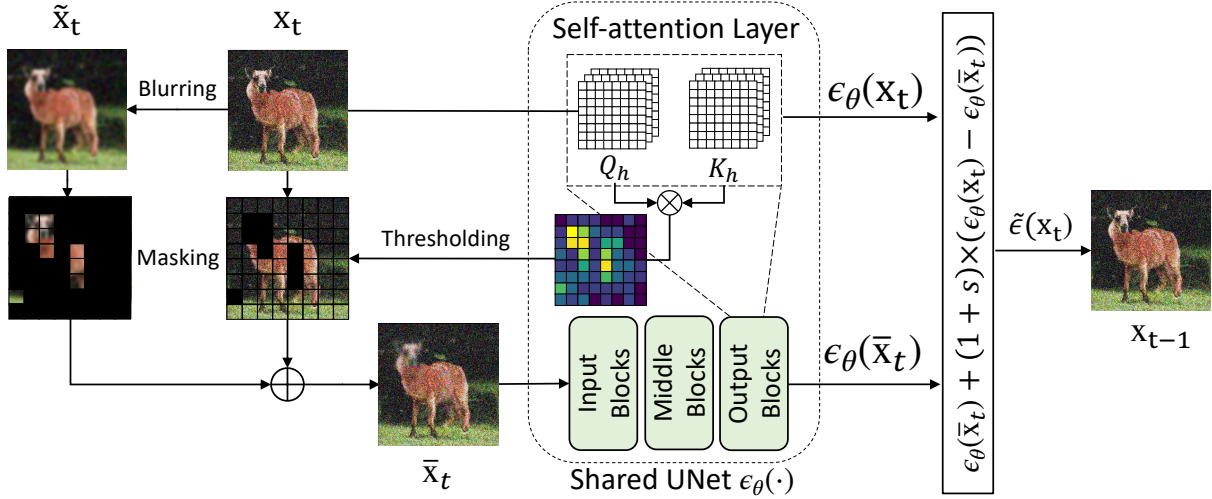


Figure 2: **Overview of our method.** First, we feed the input x_t to the UNet to get the attention map and the output $\epsilon_\theta(x_t)$. Then, we selectively mask x_t and the blurred input \tilde{x}_t according to the attention map. We combine those two to obtain \bar{x}_t , and feed it to the UNet to get $\epsilon_\theta(\bar{x}_t)$. Finally, with our guidance scale s , we linearly combine $\epsilon_\theta(\bar{x}_t)$ and $\epsilon_\theta(x_t)$ according to Eq. 17.

maps of DINO (Caron et al. 2021) to extract object masks in unsupervised semantic segmentation settings.

However, while there are some attempts to use the UNet (Ronneberger, Fischer, and Brox 2015) representation of a diffusion model (Baranchuk et al. 2021; Brempong et al. 2022), the internal self-attention maps of diffusion models are under-explored. Therefore, in this paper, we first investigate the self-attention maps within the black-boxed diffusion models and build hypotheses about them. We verify the hypotheses about the self-attention maps by conducting frequency analysis on the patches and finding the relationships with the generated objects. Through the series of intuitive experiments, we find out that the internal self-attention layers tend to focus on the high-frequency details, as well as the semantic information of the generated images. In addition to the semantic information, the high-frequency information they capture is known to be an important factor of human perception (Pianykh, Pospelova, and Kamboj 2018) and is closely related to photorealism and image quality.

To improve such image quality on diffusion models, diffusion guidance methods that use additional information such as class labels (Dhariwal and Nichol 2021; Ho and Salimans 2021) and text labels (Nichol et al. 2021) are introduced. Inspired by those, we propose a novel guidance approach, based on what the internal self-attention mechanism of diffusion models attends to, which doesn’t require an additional label, module, or training to improve image quality. It can guide diffusion models to generate images with higher fidelity by selectively blurring the patches based on the self-attention maps inside the diffusion models.

Apart from increased sample quality when used alone on the ImageNet and LSUN models, we achieve powerful results by combining our method with classifier guidance on the ImageNet 128×128 model. Also, we conduct an extensive ablation study to measure the boost performance according to varying masking strategies and guidance scales.

Related Works

Denoising Diffusion Models. Diffusion models, closely related to score-based models (Song and Ermon 2019; Song et al. 2021), have attracted much attention for their superior sampling quality. Ho *et al.* (Ho, Jain, and Abbeel 2020) proposed Denoising Diffusion Probabilistic Model (DDPM), which generates images by gradually denoising the Gaussian noise. Following this work, there are many attempts to improve the sampling process, in terms of quality and speed. Improved DDPM (Nichol and Dhariwal 2021) choose to additionally predict the variance of the reverse process of a diffusion model. DDIM (Song, Meng, and Ermon 2021) accelerates the sampling speed by introducing the non-Markovian diffusion process. Meanwhile, Latent Diffusion Model (Rombach et al. 2022) reduced the computational cost by processing the diffusion process in the latent space of the VQ-GAN (Esser, Rombach, and Ommer 2021).

Class Guidance for Diffusion Models. Recently, diffusion guidance methods based on class labels are proposed to generate images with higher quality (Dhariwal and Nichol 2021; Ho and Salimans 2021). Classifier guidance (Dhariwal and Nichol 2021) is an approach that uses a trained classifier that guides the reverse process toward a specific class distribution. Ho and Salimans (Ho and Salimans 2021) proposed classifier-free guidance, an alternative strategy for classifier guidance without the need for an additional classifier. They train a conditional model both conditionally and unconditionally by randomly substituting a class label with the null class label during the training phase. Due to its simplicity of implementation and effectiveness, this method has been widely used in high-quality diffusion models (Ramesh et al. 2022; Rombach et al. 2022; Tang et al. 2022; Wang et al. 2022; Nichol et al. 2021).

Self-Attention in Generative Models. A self-attention mechanism is the key ingredient of transformer-based mod-

els (Vaswani et al. 2017). Its expressiveness and capability to encode the long-term dependency of a sequence made it possible for the transformer model to succeed in the NLP areas. It inspired many works to incorporate this mechanism into various computer vision tasks, including image generation. Jiang *et al.* (Jiang, Chang, and Wang 2021) and Zhang *et al.* (Zhang et al. 2022, 2019) successfully incorporate self-attention into the GAN framework for better image quality. Diffusion models also adopted self-attention to their model architecture. DDPM (Ho, Jain, and Abbeel 2020) implemented self-attention layer at 16×16 resolution of UNet (Ronneberger, Fischer, and Brox 2015). Following this, Dhariwal and Nichol (Dhariwal and Nichol 2021) conducted an ablation study on the number of attention heads and the resolutions at which self-attention takes place, and improved the performance remarkably.

Internal Representations of Diffusion Models. Denoising autoencoders (Vincent et al. 2008, 2010) have been studied for a long time. The process of predicting a clean image from the noised image enables the model to learn the representations of the input data. Besides, motivated by the success of the diffusion models in the generation tasks, there are some efforts to utilize the diffusion models in other tasks, such as semantic segmentation. Brempong *et al.* (Brempong et al. 2022) showed that the denoising pretraining boosts the performance of the semantic segmentation task, and Baranchuk *et al.* (Baranchuk et al. 2021) proposed a label-efficient strategy for semantic segmentation using the UNet (Ronneberger, Fischer, and Brox 2015) representation of DDPM (Ho, Jain, and Abbeel 2020).

Preliminaries

Denoising Diffusion Probabilistic Models

Denoising Diffusion Probabilistic Models (DDPM) (Ho, Jain, and Abbeel 2020) is a generative model that generates an image from white noise with iterative denoising steps. Given an image \mathbf{x}_0 and a variance schedule β_t for an arbitrary timestep t , the forward process is defined as a Markov process of the form:

$$q(\mathbf{x}_{t+1}|\mathbf{x}_t) = \mathcal{N}(\mathbf{x}_{t+1}; \sqrt{1 - \beta_t}\mathbf{x}_t, \beta_t\mathbf{I}). \quad (1)$$

Note that we can directly get \mathbf{x}_t from \mathbf{x}_0 in the closed form:

$$q(\mathbf{x}_t|\mathbf{x}_0) = \mathcal{N}(\mathbf{x}_t; \sqrt{\bar{\alpha}_t}\mathbf{x}_0, (1 - \bar{\alpha}_t)\mathbf{I}), \quad (2)$$

where $\alpha_t = 1 - \beta_t$, and $\bar{\alpha}_t = \prod_{i=1}^t \alpha_i$. Similarly, the reverse process is defined as:

$$p_\theta(\mathbf{x}_{t-1}|\mathbf{x}_t) = \mathcal{N}(\mathbf{x}_{t-1}; \mu_\theta(\mathbf{x}_t, t), \beta_\theta(\mathbf{x}_t, t)\mathbf{I}), \quad (3)$$

where both μ_θ and β_θ are neural networks with parameter θ .

For the training phase, with β_θ fixed to a constant σ_t^2 as in DDPM (Ho, Jain, and Abbeel 2020), $p_\theta(\mathbf{x}_{t-1}|\mathbf{x}_t)$ is compared with the following forward posterior:

$$q(\mathbf{x}_{t-1}|\mathbf{x}_0, \mathbf{x}_t) = \mathcal{N}(\mathbf{x}_{t-1}; \tilde{\mu}_t(\mathbf{x}_0, \mathbf{x}_t), \tilde{\beta}_t\mathbf{I}), \quad (4)$$

where $\tilde{\mu}_t = \frac{\sqrt{\bar{\alpha}_{t-1}}\beta_t}{1 - \bar{\alpha}_t}\mathbf{x}_0 + \frac{\sqrt{\alpha_t}(1 - \bar{\alpha}_{t-1})}{1 - \bar{\alpha}_t}\mathbf{x}_t$, and $\tilde{\beta}_t = \frac{1 - \bar{\alpha}_{t-1}}{1 - \bar{\alpha}_t}\beta_t$. However, instead of directly comparing μ_θ to $\tilde{\mu}_t$,

Ho *et al.* (Ho, Jain, and Abbeel 2020) discovered that it is beneficial to optimize ϵ_θ with the following simplified objective after reparameterization:

$$\mathbf{x}_t = \sqrt{\bar{\alpha}_t}\mathbf{x}_0 + \sqrt{1 - \bar{\alpha}_t}\epsilon, \quad \text{where } \epsilon \sim \mathcal{N}(0, \mathbf{I}), \quad (5)$$

$$L_{\text{simple}} = \mathbf{E}_{\mathbf{x}_0, t, \epsilon}[\|\epsilon - \epsilon_\theta(\sqrt{\bar{\alpha}_t}\mathbf{x}_0 + \sqrt{1 - \bar{\alpha}_t}\epsilon, t)\|^2]. \quad (6)$$

For sampling $\mathbf{x}_{t-1} \sim p_\theta(\mathbf{x}_{t-1}|\mathbf{x}_t)$, we can compute:

$$\mathbf{x}_{t-1} = \frac{1}{\sqrt{\bar{\alpha}_t}}(\mathbf{x}_t - \frac{\beta_t}{\sqrt{1 - \bar{\alpha}_t}}\epsilon_\theta(\mathbf{x}_t, t)) + \sigma_t\mathbf{z}, \quad (7)$$

where $\mathbf{z} \sim \mathcal{N}(0, \mathbf{I})$. For simplicity, we denote $\epsilon_\theta(\mathbf{x}_t) := \epsilon_\theta(\mathbf{x}_t, t)$ for the rest of the paper. Rewriting Eq. 5, we can get $\hat{\mathbf{x}}_0$ which is a prediction of \mathbf{x}_0 using the following formula:

$$\hat{\mathbf{x}}_0 = (\mathbf{x}_t - \sqrt{1 - \bar{\alpha}_t}\epsilon_\theta(\mathbf{x}_t, t))/\sqrt{\bar{\alpha}_t}. \quad (8)$$

Classifier-Free Guidance

To bring capability of trading diversity for fidelity to diffusion models, Dhariwal and Nichol (Dhariwal and Nichol 2021) proposed classifier guidance that trains and uses an additional classifier module $p(c|\mathbf{x}_t)$. The guidance can be formulated as the following:

$$\tilde{\epsilon}(\mathbf{x}_t, c) = \epsilon_\theta(\mathbf{x}_t, c) - s\sqrt{1 - \bar{\alpha}_t}\nabla_{\mathbf{x}_t} \log p(c|\mathbf{x}_t), \quad (9)$$

where $s > 0$ is a scaling factor. On the other hand, Ho and Salimans (Ho and Salimans 2021) presented a classifier-free guidance strategy that can have the same effect without an additional classifier by utilizing an implicit classifier $p_{\text{implicit}}(c|\mathbf{x}_t)$. By Bayesian rule, $p_{\text{implicit}}(c|\mathbf{x}_t) \propto p(\mathbf{x}_t|c)/p(\mathbf{x}_t)$, and the score can be derived:

$$\nabla_{\mathbf{x}_t} \log p_{\text{implicit}}(c|\mathbf{x}_t) = \frac{-1}{\sqrt{1 - \bar{\alpha}_t}}(\epsilon^*(\mathbf{x}_t, c) - \epsilon^*(\mathbf{x}_t)), \quad (10)$$

where ϵ^* is the true score of the input. Combining Eq. 9 and Eq. 10, we obtain the equation for the classifier-free guidance as shown below:

$$\tilde{\epsilon}(\mathbf{x}_t, c) = \epsilon_\theta(\mathbf{x}_t, c) + s \times (\epsilon_\theta(\mathbf{x}_t, c) - \epsilon_\theta(\mathbf{x}_t)) \quad (11)$$

$$= \epsilon_\theta(\mathbf{x}_t) + (1 + s) \times (\epsilon_\theta(\mathbf{x}_t, c) - \epsilon_\theta(\mathbf{x}_t)). \quad (12)$$

However, this method still demands hard-earned class labels, a conditional model to apply the guidance, and additional training details.

Self-Attention in Diffusion Models

Several works of diffusion models uses the UNet (Ronneberger, Fischer, and Brox 2015) structure with self-attention (Vaswani et al. 2017) at one or some of the intermediate layers (Ho, Jain, and Abbeel 2020; Dhariwal and Nichol 2021). Specifically, for the height H and width W , given any feature map $X \in \mathbb{R}^{(HW) \times C}$ at a layer l , the N -head self-attention map is defined as:

$$Q_h = XW_h^Q, \quad K_h = XW_h^K, \quad (13)$$

$$A_h = \text{softmax}(Q_hK_h^T/\sqrt{d}), \quad (14)$$

where $W_h^Q, W_h^K \in \mathbb{R}^{C \times d}$ for $h = 0, 1, \dots, N - 1$. The attention map is then right multiplied by $V_h = XW_h^V$ with $W_h^V \in \mathbb{R}^{C \times d}$ and projected to the same channel as the input to produce the output.



Figure 3: **Comparison of self-attention masks.** (a) Self-attention masks of DINO (Caron et al. 2021), (b) self-attention masks of unconditional ADM (Dhariwal and Nichol 2021). Compared to the self-attention masks of the DINO, those of ADM tend to attend to the high-frequency details, *e.g.*, edge of an object, bushes, pebbles, and other repetitive patterns, rather than being centric on a single object.

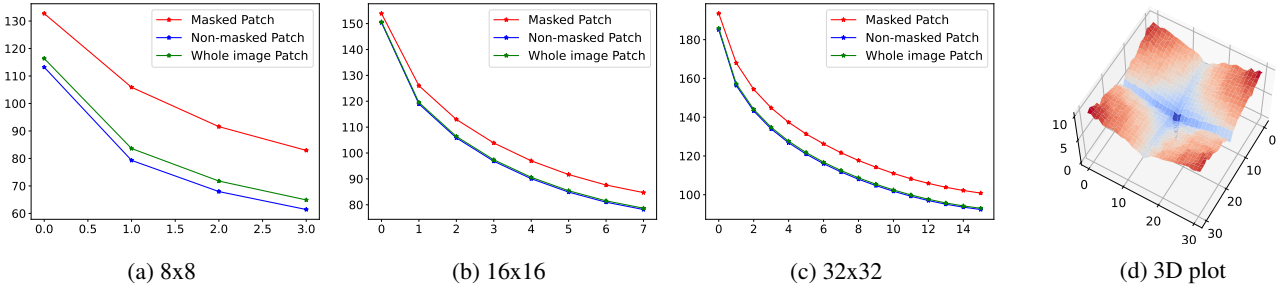


Figure 4: **Frequency analysis of the attention masks.** (a), (b) and (c) show the frequency magnitude comparison of 8×8 , 16×16 , and 32×32 patch sizes, respectively. The last-layer attention maps of the corresponding resolution are used to extract the masks. (d) is the 3D visualization of the percentage of magnitude difference between the attention masks and the inverted masks regarding the 32×32 patches.

Exploring Properties of Self-Attention in Diffusion Models

Although some literature utilized UNet (Ronneberger, Fischer, and Brox 2015) feature maps of diffusion models for label-efficient semantic segmentation (Baranchuk et al. 2021; Brempong et al. 2022), analyzing and utilizing the self-attention maps inside diffusion models remain under-explored. In this section, by conducting experiments with those self-attention maps, we carefully examine the regions to which the self-attention in a diffusion model attends.

Our Hypotheses

First of all, we hypothesize concerning the internal self-attention maps of diffusion models that 1) the self-attention maps attend to the high-frequency details, and 2) they are also related to the semantic information, such as objects in the generated images. In the following, we visualize the self-attention maps in comparison to the vision transformer (Dosovitskiy et al. 2021) trained in the self-supervised manner, and subsequently set and conduct intuitive experiments to verify our hypotheses.

Visualization of Self-Attention

Similar to training unconditional diffusion models (Ho, Jain, and Abbeel 2020), self-supervised learning (Caron et al. 2021) does not require labels to learn the internal representation. Caron *et al.* (Caron et al. 2021) showed that the self-attention maps of the self-supervised transformer are themselves object-oriented and effective for the downstream tasks such as semantic segmentation and video object segmentation. In the assumption that the self-attention module in the diffusion UNet (Ronneberger, Fischer, and Brox 2015) can act like DINO (Caron et al. 2021), we decide to visualize this representation. In the experiments, we conduct Global Average Pooling (GAP) to aggregate the attention map of ADM (Dhariwal and Nichol 2021) in Eq. 14. The last self-attention module in the unconditional ImageNet model of ADM (Dhariwal and Nichol 2021) is used to extract the attention maps, which are then averaged along the heads and timesteps and then thresholded as in DINO (Caron et al. 2021) to produce the attention mask.

Frequency Analysis on Self-Attention

Compared to the self-attention maps of the last layer of ViT (Dosovitskiy et al. 2021) trained by DINO (Caron et al.

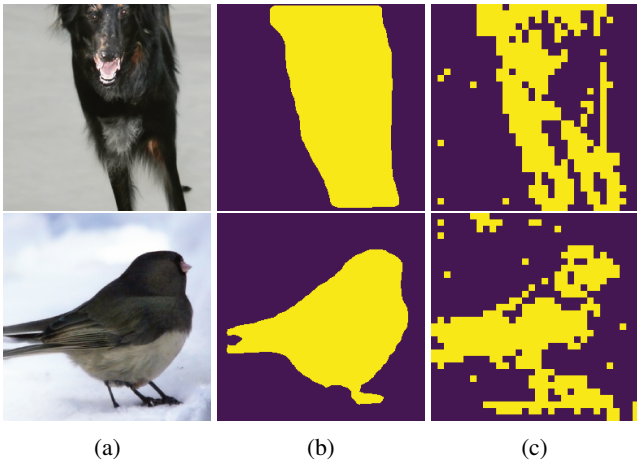


Figure 5: **Visualization of self-attention masks compared to object masks.** (a) Generated images, (b) the object masks of Mask R-CNN (He et al. 2017) (c) the self-attention masks of unconditional ADM (Dhariwal and Nichol 2021).

Map size	Random	Self-attn.
8×8	0.19	0.27
16×16	0.18	0.26
32×32	0.16	0.23

Table 1: Intersection of Unit (IoU) between the object mask predicted by off-the-shelf Mask R-CNN (He et al. 2017) and the self-attention of diffusion models.

2021) in Fig. 3, those of ADM (Dhariwal and Nichol 2021) are distinguishable. An interesting characteristic of the attention module inside the diffusion model is that it is attending to the edge and other high-frequency details, *e.g.*, bushes, pebbles, and faces. In contrast to DINO (Caron et al. 2021) whose self-attention map is clearly object-centric, it is indeed focusing on the objects but hardly on the textureless (*i.e.* low-frequency) part of the object.

In this insight, we conduct frequency analysis on the patches with respect to the attention mask. We perform the 2D fast Fourier transform (FFT) to the patches of generated images to extract the frequency maps. The frequency-magnitude visualization of the maps is in Fig. 4. We use the last self-attention modules of each resolution containing them in ADM (Dhariwal and Nichol 2021), *i.e.*, 8×8 , 16×16 , and 32×32 .

It demonstrates that the masked patches, which have a high attention score, have relatively higher frequency than the unmasked counterparts. With these experimental results, we can say that the masking based on the self-attention map of a diffusion model can effectively capture the high-frequency region.

Semantic Analysis on Self-Attention

While the self-attention heads are hardly focusing on the textureless part of the object, we find out that they also tend to focus on the semantic information. To measure this



Figure 6: **Unstability of the blur guidance.** Given a large guidance scale, the blur guidance generates unstable images (top row) compared to the self-attention guidance (bottom row).

quantitatively, we use off-the-shelf Mask R-CNN (He et al. 2017) pretrained with COCO 2017 dataset (Lin et al. 2014) to get the semantic mask and compute Intersection of Unit (IoU) with the self-attention mask of a diffusion model. We obtained attention masks from the unconditional ImageNet model of ADM (Dhariwal and Nichol 2021) in the same way as the subsection above. Counterparts are set to randomly predict the same number of pixels. The result is shown in Table 1.

Although the masks generated by self-attention maps in diffusion models are not complete, they capture general semantic information like an object and its shadow (Fig. 5), and the tendency for the self-attention maps to focus on the semantic information exists across attention maps at all resolutions (Table 1).

Utilizing the Self-Attention Map to Improve Sample Quality

One of the limitations of existing guidance methods is that they require image labels (Dhariwal and Nichol 2021; Ho and Salimans 2021). Besides, a conditional model, classifier, or CLIP (Radford et al. 2021) must be trained additionally. In this section, we propose self-attention guidance, which is inference-time guidance applicable to any kind of pretrained diffusion model, *i.e.*, conditional and unconditional, utilizing the internal self-attention of the diffusion model itself. The overview of our method is shown in Fig. 2.

Blur Guidance for Diffusion Models

High-frequency information such as faces, texture, and the edge of an object has a huge contribution to human perception (Pianykh, Pospelova, and Kamboj 2018). Intentionally disrupting diffusion models to make predictions not conditioned on such high-frequency information with Gaussian blur, and giving guidance, which we call the *blur guidance* in this subsection, to the conditional ones help the models to develop the high-frequency information further. Intuitively, while the classifier-free guidance (Ho and Salimans 2021) utilizes the less-informed unconditional prediction, the blur guidance utilizes the less-informed prediction of the blurred image to provide the direction of the guidance. Note that

Model	# of steps	Self-attention guidance scale	FID	sFID	IS	Precision	Recall
ImageNet 256×256 (Uncond.)	250	0.0 (no guidance)	26.21	6.35	39.70	0.61	0.63
		0.5	<u>20.31</u>	5.09	<u>45.30</u>	<u>0.66</u>	<u>0.61</u>
		0.8	20.08	<u>5.77</u>	45.56	0.68	0.59
ImageNet 256×256 (Cond.)	250	0.0 (no guidance)	10.94	6.02	100.98	0.69	0.63
		0.2	9.41	5.28	104.79	0.70	0.62
LSUN Cat 256×256	250	0.0 (no guidance)	7.03	8.24	-	0.60	0.53
		0.05	6.87	8.21	-	0.60	0.50
LSUN Horse 256×256	250	0.0 (no guidance)	3.45	7.55	-	0.68	0.56
		0.01	3.43	7.51	-	0.68	0.55

Table 2: Self-attention guidance on pretrained ADMs.

SAG	CG	FID	sFID	Precision	Recall
		5.91	5.09	0.70	0.65
	✓	2.97	5.09	0.78	0.59
✓		5.11	4.09	0.72	0.65
✓	✓	2.58	4.35	0.79	0.59

Table 3: Compatibility of self-attention guidance with classifier guidance. SAG denotes the self-attention guidance and CG denotes the classifier guidance.

Gaussian blur is an appropriate method for pretrained diffusion models since its output does not significantly deviate from the original image, while suppressing high-frequency signals.

Using the Gaussian filter, Gaussian blur is applied to an image with a kernel size k and standard deviation σ . As in a similar form to Eq. 12, the blur guidance is formulated as the following during sampling time:

$$\tilde{\epsilon}(\mathbf{x}_t) = \epsilon_\theta(\tilde{\mathbf{x}}_t) + (1 + s) \times (\epsilon_\theta(\mathbf{x}_t) - \epsilon_\theta(\tilde{\mathbf{x}}_t)), \quad (15)$$

where $\tilde{\mathbf{x}}_t$ is the blurred version of \mathbf{x}_t , and the scalar $s > 0$ is the guidance scale. To condition the guidance on the content, and not on the random noise, $\hat{\mathbf{x}}_0$ at Eq. 8 is blurred and diffused again with the noise $\epsilon_\theta(\mathbf{x}_t)$ to produce $\tilde{\mathbf{x}}_t$. Since \mathbf{x}_t contains higher frequency details than $\tilde{\mathbf{x}}_t$, the sampling process is guided toward the image that utilizes the information.

However, the blur guidance has an issue when directly applied to existing methods. Since blur is applied globally, the network output is not conditioned on any single pixel. Therefore, the prediction is entirely different from that of an original image. In addition, degradation of sampled images occurs (Fig. 6), since the guidance also unstabilizes the pixels of unnecessary components like background or smooth regions.

Self-Attention Guidance for Diffusion Models

Based on the findings in the fourth section, we can say that the internal UNet (Ronneberger, Fischer, and Brox 2015) self-attention maps of diffusion models tend to focus on high-frequency details while capturing the semantic cluster. These characteristics are aligned with those of

human perception, *i.e.*, photorealism, since it also relies on high-frequency information (Pianykh, Pospelova, and Kamboj 2018) and semantic meaning. Selectively blurring the patches where diffusion models attend disturbs the model developing the details needed for such photorealism. Therefore, given the guidance from the disabled to the clean, the model gets to elaborate on them. The problem of the blur guidance stated above is effectively avoided, since it is conditioned on unmasked pixels and locally guides informative patches that get to represent high-frequency details and semantically meaningful contents as shown below.

Generalizing Eq. 15, given a mask M obtained in the same manner as in the fourth section, the self-attention guidance blurs only the masked patches of \mathbf{x}_t and is formulated as follows:

$$\bar{\mathbf{x}}_t = (1 - M) \odot \mathbf{x}_t + M \odot \tilde{\mathbf{x}}_t, \quad (16)$$

$$\tilde{\epsilon}(\mathbf{x}_t) = \epsilon_\theta(\bar{\mathbf{x}}_t) + (1 + s) \times (\epsilon_\theta(\mathbf{x}_t) - \epsilon_\theta(\bar{\mathbf{x}}_t)). \quad (17)$$

where \odot denotes the Hadamard product. Different from the blur guidance, $\epsilon(\bar{\mathbf{x}}_t)$ can be interpreted explicitly to be conditioned on the unmasked patches:

$$\tilde{\epsilon}(\mathbf{x}_t) = \epsilon_\theta(\dot{\mathbf{x}}_t, \bar{\mathbf{y}}_t) + (1 + s) \times (\epsilon_\theta(\dot{\mathbf{x}}_t, \mathbf{y}_t) - \epsilon_\theta(\dot{\mathbf{x}}_t, \bar{\mathbf{y}}_t)), \quad (18)$$

where $\dot{\mathbf{x}}_t = (1 - M) \odot \mathbf{x}_t$, $\mathbf{y}_t = M \odot \mathbf{x}_t$, and $\bar{\mathbf{y}}_t = M \odot \bar{\mathbf{x}}_t$. Again, note for the resemblance with Eq. 12. Destroyed high-frequency and semantic information of the selected patches by Gaussian blur in Eq. 18 act as a class label in Eq. 12.

Experimental Results

We build upon ADM (Dhariwal and Nichol 2021), and we use the publically available checkpoints from the repository. In the first subsection, we evaluate the self-attention guidance on conditional and unconditional models pretrained on ImageNet (Deng et al. 2009) 256×256, and LSUN (Yu et al. 2015) Cat and Horse. In the following subsection, we test our method combined with the classifier guidance (Dhariwal and Nichol 2021) to show the compatibility with classifier guidance (Dhariwal and Nichol 2021). Subsequently, we conduct extensive ablation studies to verify the effectiveness of our method and justify our choices. For a fair comparison, following ADM (Dhariwal and Nichol 2021), we use

Masking strategy	FID	IS
Baseline	5.98	141.72
Global	5.82	143.15
Random	5.68	148.99
Square	5.68	146.50
Self-attention	5.47	151.12
DINO-attention	5.63	146.18

Table 4: Ablation study of the masking strategy.

Mask Threshold	FID	IS
Baseline	5.98	141.72
0.7	5.67	148.60
1.0	5.47	151.12
1.3	5.66	145.58

Table 5: Ablation study of the attention mask threshold.

the same evaluation metrics including Fréchet inception distance (FID) (Heusel et al. 2017), sFID (Nash et al. 2021), Inception Score (IS) (Salimans et al. 2016), and Improved Precision and Recall (Kynkäänniemi et al. 2019).

Results on the Pretrained Models

We show the evaluation results of our method with the pre-trained models of ADM (Dhariwal and Nichol 2021) at ImageNet 256×256, LSUN Cat, and LSUN Horse in this section. The scale of classifier guidance is set to 0 in this experiment.

As shown in Table 2, we observe that our method improves the fidelity of conditional and unconditional ImageNet models, across all the evaluation metrics except for the recall. For LSUN Cat and Horse models, applying our method also make the models obtain higher FID and sFID. We observe a relatively lower recall score shown in (Dhariwal and Nichol 2021; Ho and Salimans 2021), which can be interpreted as an inevitable trade-off between sample fidelity and diversity. Note that while the application of classifier guidance (Dhariwal and Nichol 2021) is limited to the labeled dataset, we can apply self-attention guidance to unlabeled datasets, *e.g.*, ImageNet without labels, or LSUN.

Compatibility with Classifier Guidance

Although self-attention guidance is designed for unconditional and unguided models, we can combine it with the existing method, classifier guidance (Dhariwal and Nichol 2021). To this end, we test four cases to use the guidance, with or without classifier guidance and self-attention guidance. The metrics are evaluated on 50K samples generated by the ImageNet 128×128 model. As shown in Table 3, we can find that additional improvements on the FID and precision are made when using both of them. This result implies that the proposed guidance which is unconditional to image labels, can be used simultaneously with the conditional guidance methods.

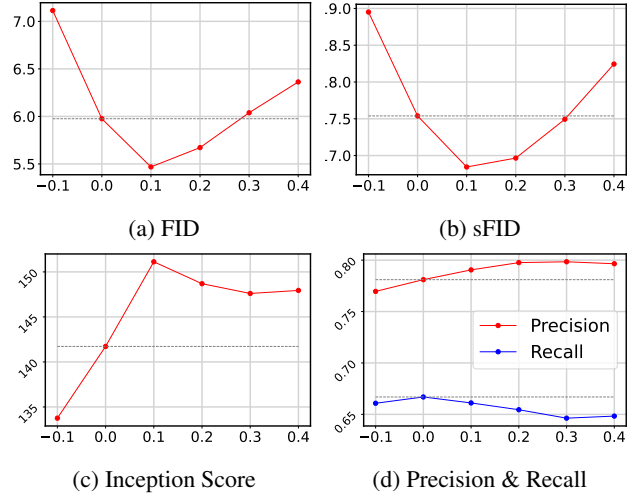


Figure 7: **Ablation study of the guidance scale.** The x-axis denotes the guidance scale, and the dotted line denotes the performance of the baseline, *i.e.* the model without self-attention guidance.

Layer	FID	IS
Baseline	5.98	141.72
Out. 2	5.59	150.62
Out. 5	5.57	141.73
Out. 8	5.47	151.12

Table 6: Ablation study of the layer where we extract the attention map. *Out.* denotes the output blocks of UNet.

Ablation Study

We conduct an ablation study on the masking strategy and guidance scale to validate the effectiveness of our method. All the ablation study is performed in the conditional ImageNet 128×128 setting, and the metrics are calculated with 10K images.

Masking strategy. First, we test various masking strategies to verify the effectiveness of our self-attention masking in improving sample quality. Those strategies are used to selectively blur and give guidance to the image at each timestep. For a fair comparison, we mask 40% of the pixels of the image for the other masking experiments, which is the equivalent portion of the masking area to the self-attention masking when the threshold is 1.0. The results are shown in Table 4. We find that the self-attention masking strategy outperforms other masking strategies, *e.g.*, global, random, or square masking. Especially, applying the global masking, equivalent to blur guidance, shows the worst performance among the masking strategies, which validates the motivation for our self-attention guidance. Also, applying the mask of DINO (Caron et al. 2021) shows worse performance than our method in terms of FID and IS. Therefore, this result indicates that self-attention masking is a sufficiently effective method that produces high sample quality.

Next, we conduct experiments on the threshold of attention masking, which affects the ratio of the blurred region. We set the guidance scale as 1.1, and test the masking threshold of 0.7, 1.0, 1.3. As shown in Table 5, the highest metrics are obtained when the threshold value is 1.0.

Finally, the comparison of the extraction layers of the attention map is shown in Table 6. Following (Baranchuk et al. 2021) that used the decoder representations for semantic segmentation, we select the last self-attention layers of each resolution from the decoder, *i.e.*, 8×8 , 16×16 , and 32×32 . Regardless of the extracted layer, the performance is consistently improved, while the result of the 32×32 resolution gives the best FID and IS.

Guidance scale. We also compare the performance changes as the guidance scale changes. As shown in Fig. 7, we test the self-attention guidance scales of -0.1 , 0.1 , 0.2 , 0.3 , and 0.4 to ADM (Dhariwal and Nichol 2021) and obtain the best FID, sFID, and Inception Score at the guidance scale $s = 0.1$. The Precision metric shows the best results when the guidance scale is $s = 0.3$. We also find out that applying self-attention guidance with a negative scale ($s = -0.1$) or with a too large scale ($s \geq 0.4$) has negative effects on the sample quality.

Conclusion

In this paper, we carefully inspected the intermediate self-attention map of diffusion models and found out that diffusion models attend to the high-frequency and semantically informative patches of generated images. By selectively blurring the patches based on those self-attention maps and giving guidance, we showed improved sample quality on the ImageNet and LSUN benchmarks. In the end, we found that from unconditional diffusion models to conditional and guided ones, our methods can be directly applied without any additional training. We are looking forward to further studying our method.

References

Baranchuk, D.; Rubachev, I.; Voynov, A.; Khrulkov, V.; and Babenko, A. 2021. Label-efficient semantic segmentation with diffusion models. *arXiv preprint arXiv:2112.03126*.

Brempong, E. A.; Kornblith, S.; Chen, T.; Parmar, N.; Minderer, M.; and Norouzi, M. 2022. Denoising Pretraining for Semantic Segmentation. In *Proceedings of the IEEE/CVF Conference on Computer Vision and Pattern Recognition*, 4175–4186.

Caron, M.; Touvron, H.; Misra, I.; Jégou, H.; Mairal, J.; Bojanowski, P.; and Joulin, A. 2021. Emerging properties in self-supervised vision transformers. In *Proceedings of the IEEE/CVF International Conference on Computer Vision*, 9650–9660.

Deng, J.; Dong, W.; Socher, R.; Li, L.-J.; Li, K.; and Fei-Fei, L. 2009. Imagenet: A large-scale hierarchical image database. In *2009 IEEE Conference on Computer Vision and Pattern Recognition*, 248–255. Ieee.

Dhariwal, P.; and Nichol, A. 2021. Diffusion models beat gans on image synthesis. *Advances in Neural Information Processing Systems*, 34: 8780–8794.

Dosovitskiy, A.; Beyer, L.; Kolesnikov, A.; Weissenborn, D.; Zhai, X.; Unterthiner, T.; Dehghani, M.; Minderer, M.; Heigold, G.; Gelly, S.; et al. 2021. An image is worth 16×16 words: Transformers for image recognition at scale. In *International Conference on Learning Representations*.

Esser, P.; Rombach, R.; and Ommer, B. 2021. Taming transformers for high-resolution image synthesis. In *Proceedings of the IEEE/CVF Conference on Computer Vision and Pattern Recognition*, 12873–12883.

Goodfellow, I.; Pouget-Abadie, J.; Mirza, M.; Xu, B.; Warde-Farley, D.; Ozair, S.; Courville, A.; and Bengio, Y. 2014. Generative adversarial nets. *Advances in Neural Information Processing Systems*, 27.

Gu, S.; Chen, D.; Bao, J.; Wen, F.; Zhang, B.; Chen, D.; Yuan, L.; and Guo, B. 2022. Vector quantized diffusion model for text-to-image synthesis. In *Proceedings of the IEEE/CVF Conference on Computer Vision and Pattern Recognition*, 10696–10706.

He, K.; Gkioxari, G.; Dollár, P.; and Girshick, R. 2017. Mask r-cnn. In *Proceedings of the IEEE International Conference on Computer Vision*, 2961–2969.

Heusel, M.; Ramsauer, H.; Unterthiner, T.; Nessler, B.; and Hochreiter, S. 2017. Gans trained by a two time-scale update rule converge to a local nash equilibrium. *Advances in Neural Information Processing Systems*, 30.

Ho, J.; Jain, A.; and Abbeel, P. 2020. Denoising diffusion probabilistic models. *Advances in Neural Information Processing Systems*, 33: 6840–6851.

Ho, J.; Saharia, C.; Chan, W.; Fleet, D. J.; Norouzi, M.; and Salimans, T. 2022. Cascaded Diffusion Models for High Fidelity Image Generation. *Journal of Machine Learning Research*, 23(47): 1–33.

Ho, J.; and Salimans, T. 2021. Classifier-Free Diffusion Guidance. In *NeurIPS 2021 Workshop on Deep Generative Models and Downstream Applications*.

Jiang, Y.; Chang, S.; and Wang, Z. 2021. Transgan: Two pure transformers can make one strong gan, and that can scale up. *Advances in Neural Information Processing Systems*, 34: 14745–14758.

Kynkäänniemi, T.; Karras, T.; Laine, S.; Lehtinen, J.; and Aila, T. 2019. Improved precision and recall metric for assessing generative models. *Advances in Neural Information Processing Systems*, 32.

Lin, T.-Y.; Maire, M.; Belongie, S.; Hays, J.; Perona, P.; Ramanan, D.; Dollár, P.; and Zitnick, C. L. 2014. Microsoft coco: Common objects in context. In *European Conference on Computer Vision*, 740–755. Springer.

Nash, C.; Menick, J.; Dieleman, S.; and Battaglia, P. 2021. Generating images with sparse representations. In *International Conference on Machine Learning*, 7958–7968. PMLR.

- Nichol, A.; Dhariwal, P.; Ramesh, A.; Shyam, P.; Mishkin, P.; McGrew, B.; Sutskever, I.; and Chen, M. 2021. Glide: Towards photorealistic image generation and editing with text-guided diffusion models. *arXiv preprint arXiv:2112.10741*.
- Nichol, A. Q.; and Dhariwal, P. 2021. Improved denoising diffusion probabilistic models. In *International Conference on Machine Learning*, 8162–8171. PMLR.
- Paszke, A.; Gross, S.; Massa, F.; Lerer, A.; Bradbury, J.; Chanan, G.; Killeen, T.; Lin, Z.; Gimelshein, N.; Antiga, L.; et al. 2019. Pytorch: An imperative style, high-performance deep learning library. *Advances in Neural Information Processing Systems*, 32.
- Pianykh, O. S.; Pospelova, K.; and Kamboj, N. H. 2018. Modeling human perception of image quality. *Journal of Digital Imaging*, 31(6): 768–775.
- Radford, A.; Kim, J. W.; Hallacy, C.; Ramesh, A.; Goh, G.; Agarwal, S.; Sastry, G.; Askell, A.; Mishkin, P.; Clark, J.; et al. 2021. Learning transferable visual models from natural language supervision. In *International Conference on Machine Learning*, 8748–8763. PMLR.
- Ramesh, A.; Dhariwal, P.; Nichol, A.; Chu, C.; and Chen, M. 2022. Hierarchical text-conditional image generation with clip latents. *arXiv preprint arXiv:2204.06125*.
- Rombach, R.; Blattmann, A.; Lorenz, D.; Esser, P.; and Ommer, B. 2022. High-resolution image synthesis with latent diffusion models. In *Proceedings of the IEEE/CVF Conference on Computer Vision and Pattern Recognition*, 10684–10695.
- Ronneberger, O.; Fischer, P.; and Brox, T. 2015. U-net: Convolutional networks for biomedical image segmentation. In *International Conference on Medical image computing and computer-assisted intervention*, 234–241. Springer.
- Salimans, T.; Goodfellow, I.; Zaremba, W.; Cheung, V.; Radford, A.; and Chen, X. 2016. Improved techniques for training gans. *Advances in Neural Information Processing Systems*, 29.
- Song, J.; Meng, C.; and Ermon, S. 2021. Denoising Diffusion Implicit Models. In *International Conference on Learning Representations*.
- Song, Y.; and Ermon, S. 2019. Generative modeling by estimating gradients of the data distribution. *Advances in Neural Information Processing Systems*, 32.
- Song, Y.; Sohl-Dickstein, J.; Kingma, D. P.; Kumar, A.; Ermon, S.; and Poole, B. 2021. Score-based generative modeling through stochastic differential equations. In *International Conference on Learning Representations*.
- Tang, Z.; Gu, S.; Bao, J.; Chen, D.; and Wen, F. 2022. Improved Vector Quantized Diffusion Models. *arXiv preprint arXiv:2205.16007*.
- Van Gansbeke, W.; Vandenhende, S.; and Van Gool, L. 2022. Discovering Object Masks with Transformers for Unsupervised Semantic Segmentation. *arXiv preprint arXiv:2206.06363*.
- Vaswani, A.; Shazeer, N.; Parmar, N.; Uszkoreit, J.; Jones, L.; Gomez, A. N.; Kaiser, Ł.; and Polosukhin, I. 2017. Attention is all you need. *Advances in Neural Information Processing Systems*, 30.
- Vincent, P.; Larochelle, H.; Bengio, Y.; and Manzagol, P.-A. 2008. Extracting and composing robust features with denoising autoencoders. In *Proceedings of the 25th International Conference on Machine Learning*, 1096–1103.
- Vincent, P.; Larochelle, H.; Lajoie, I.; Bengio, Y.; and Manzagol, P.-A. 2010. Stacked Denoising Autoencoders: Learning Useful Representations in a Deep Network with a Local Denoising Criterion. *Journal of Machine Learning Research*, 11: 3371–3408.
- Wang, T.; Zhang, T.; Zhang, B.; Ouyang, H.; Chen, D.; Chen, Q.; and Wen, F. 2022. Pretraining is All You Need for Image-to-Image Translation. *arXiv preprint arXiv:2205.12952*.
- Yu, F.; Seff, A.; Zhang, Y.; Song, S.; Funkhouser, T.; and Xiao, J. 2015. Lsun: Construction of a large-scale image dataset using deep learning with humans in the loop. *arXiv preprint arXiv:1506.03365*.
- Zadaianchuk, A.; Kleindessner, M.; Zhu, Y.; Locatello, F.; and Brox, T. 2022. Unsupervised Semantic Segmentation with Self-supervised Object-centric Representations. *arXiv preprint arXiv:2207.05027*.
- Zhang, B.; Gu, S.; Zhang, B.; Bao, J.; Chen, D.; Wen, F.; Wang, Y.; and Guo, B. 2022. Styleswin: Transformer-based gan for high-resolution image generation. In *Proceedings of the IEEE/CVF Conference on Computer Vision and Pattern Recognition*, 11304–11314.
- Zhang, H.; Goodfellow, I.; Metaxas, D.; and Odena, A. 2019. Self-attention generative adversarial networks. In *International Conference on Machine Learning*, 7354–7363. PMLR.

Appendix A. Additional Implementation Details.

Environmental setting

For all the experiments, we use 2 servers with 8 NVIDIA GeForce RTX 3090 GPUs each to sample from pretrained models of ADM (Dhariwal and Nichol 2021). We build upon the PyTorch (Paszke et al. 2019) implementation of ADM (Dhariwal and Nichol 2021), and all the weights for our experiments are taken from their publicly available repository.

Implementation details

Since we only use the sampling stage of the diffusion model, we follow the sampling setting of ADM (Dhariwal and Nichol 2021). We use 250 uniform sampling steps for all the qualitative and quantitative experiments in the main paper and this supplementary material, and we apply our self-attention guidance to every step except for Fig. 1.

Hyperparameter settings

We report our hyperparameter settings for our experiments in Table 7. For Fourier and semantic analysis, we use the unconditional model of ADM (Dhariwal and Nichol 2021) and get the mask with threshold 1. For the visualizing experiment in comparison to DINO (Caron et al. 2021), we use a thresholding method proposed in DINO (Caron et al. 2021), which keeps a certain percentage of the mass of the self-attention maps at the last layer. In addition, we use the last attention layer of UNet (Ronneberger, Fischer, and Brox 2015) decoder to get the attention map in the same resolution as DINO (Caron et al. 2021). In the ablation study, while testing the ablated parameter, we set the other parameters to constants.

Model	Self-attention parameter			Gaussian-blur parameter	
	Guidance scale	Threshold	Layer	σ	k
ImageNet 256×256 (unconditional, analysis)	-	1.0	{Output 2, Output 5, Output 8}	-	-
ImageNet 256×256 (unconditional)	0.5, 0.8	1.0	Output 2	9	31
ImageNet 256×256 (conditional)	0.2	1.0	Output 2	9	31
LSUN Cat 256×256	0.05	1.0	Output 2	9	31
LSUN Horse 256×256	0.01	1.0	Output 2	9	31
ImageNet 128×128	0.1	1.0	Output 8	3	31
ImageNet 128×128 (abl.)	{-0.1, 0.1, 0.2, 0.3}	1.0	Output 8	3	31
	0.1	{0.7, 1.0, 1.3}	Output 8	3	31
	0.1	1.0	{Output 2, Output 5, Output 8}	3	31

Table 7: Hyperparameter settings. *abl.* denotes hyperparameters used in ablation studies.

Appendix B. Additional Results and Analysis

Visualization of attention maps

We show the visualizations of self-attention maps in the all 8×8 , 16×16 , and 32×32 resolutions of UNet (Ronneberger, Fischer, and Brox 2015) in Fig. 8. The attention maps at $t = 0, 49, 99, 149, 199, 249$ are visualized at each row in order, and the layers are aligned left to right in order. We can see that the attention maps at the intermediate timesteps capture the structure of generated images.

In addition, we extract the self-attention masks from the different heads and layers from the UNet (Ronneberger, Fischer, and Brox 2015) and visualized them in Fig. 9 and Fig. 10. We follow the visualization method from DINO (Caron et al. 2021). *Average* in this figure means the obtained masks after averaging attention maps of the four heads. As described in the main paper, they tend to capture high-frequency and semantically meaningful patches.

Additional ablation study

In the main paper, we conduct an ablation study of the output layers at which the attention maps are extracted following (Baranchuk et al. 2021). Additionally, in this supplementary material, we show another ablation study for the attention maps from input and middle blocks of UNet (Ronneberger, Fischer, and Brox 2015), and the result is shown in Table 8. We use the last self-attention module among the same resolution because the last layers can see the aggregated representation of the

former layers. The 8th and 11th layers of the input blocks are the last layer of each 32×32 and 16×16 resolution, respectively, and we denote the n th layer of the input blocks as *In. n* in the table. Wherever attention maps are extracted, our method shows the increase in terms of FID and IS compared to the baseline.

Layer	FID	IS
Baseline	5.98	141.72
In. 8	5.61	148.20
In. 11	5.54	150.07
Mid.	5.63	143.44

Table 8: Ablation study of the layer where we extract the attention map. *In.* and *Mid.* denotes the input and middle blocks of UNet (Ronneberger, Fischer, and Brox 2015), respectively.

Next, we study the parameter of the Gaussian blur. For the fixed kernel size $k = 31$, we tested $\sigma \in \{1, 3, 9\}$. For the resolution of 128×128 , setting the $\sigma = 3$ shows the best performance in our method. Note that the effect of the sigma σ is dependent on the input resolution.

σ	FID	IS
Baseline	5.98	141.72
1	5.58	145.85
3	5.47	151.12
9	5.70	148.70

Table 9: Ablation study of the sigma(σ) of Gaussian-blur.

Computational efficiency

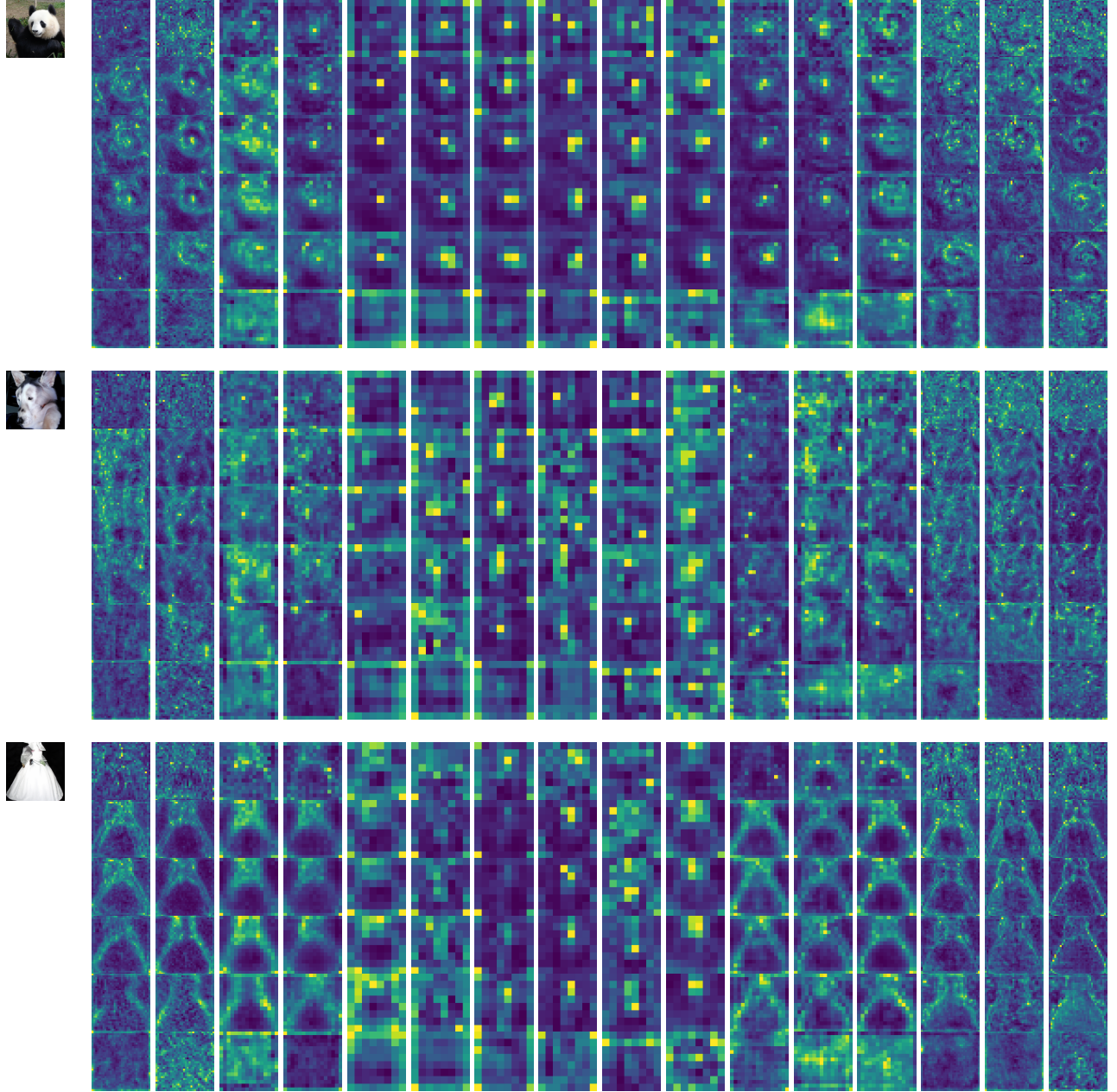
In this section, we report the computational cost in the table below. The allocated GPU memory and sampling time for sampling a mini-batch of 16 samples from the ImageNet (Deng et al. 2009) 256×256 model using a single NVIDIA RTX 3090 GPU are reported. The sampling time for 50k samples with the GPU is also reported below. *SAG* denotes our method, self-attention guidance, and *CG* denotes classifier guidance (Dhariwal and Nichol 2021). Being the same problem as classifier-free guidance (Ho and Salimans 2021), an additional feedforward step is conducted to get the direction of the guidance. On the other hand, the increase in memory usage is only about 2.4%, which shows the advantage of not engaging other modules in our method compared to classifier guidance (Dhariwal and Nichol 2021).

	SAG + CG	CG
Allocated GPU memory	17146MB	16750MB
Sampling Time	9m 41s	5m 46s
Sampling Time (50k samples)	2d 16h	1d 14h

Table 10: Comparison of computational cost between Self Attention Guidance (SAG) and Classifier Guidance (CG).

Qualitative results

We provide the results from ImageNet (Deng et al. 2009) 128×128 conditional model with our method in Fig. 11, and the results from LSUN Cat (Yu et al. 2015) with our method in Fig. 12. Also, in addition to the Fig. 1 in the main paper, we show the more comparisons of unselected samples from the unconditional ImageNet (Deng et al. 2009) 256×256 model in Fig. 13. We report each result with the same seed for comparison. From these results, we can show that applying our method can improve the fine details *e.g.*, the texture of food, human faces, or the details of animals.



In. 7 In. 8 In. 10 In. 11 In. 13 In. 14 Mid. Out. 0 Out. 1 Out. 2 Out. 3 Out. 4 Out. 5 Out. 6 Out. 7 Out. 8

Figure 8: **Examples of attention maps of all self-attention layers of ADM (Dhariwal and Nichol 2021).** In. n , Mid., and Out. n denote the attention map of the n th block of the input blocks, the middle block, and the n th block of the output blocks.

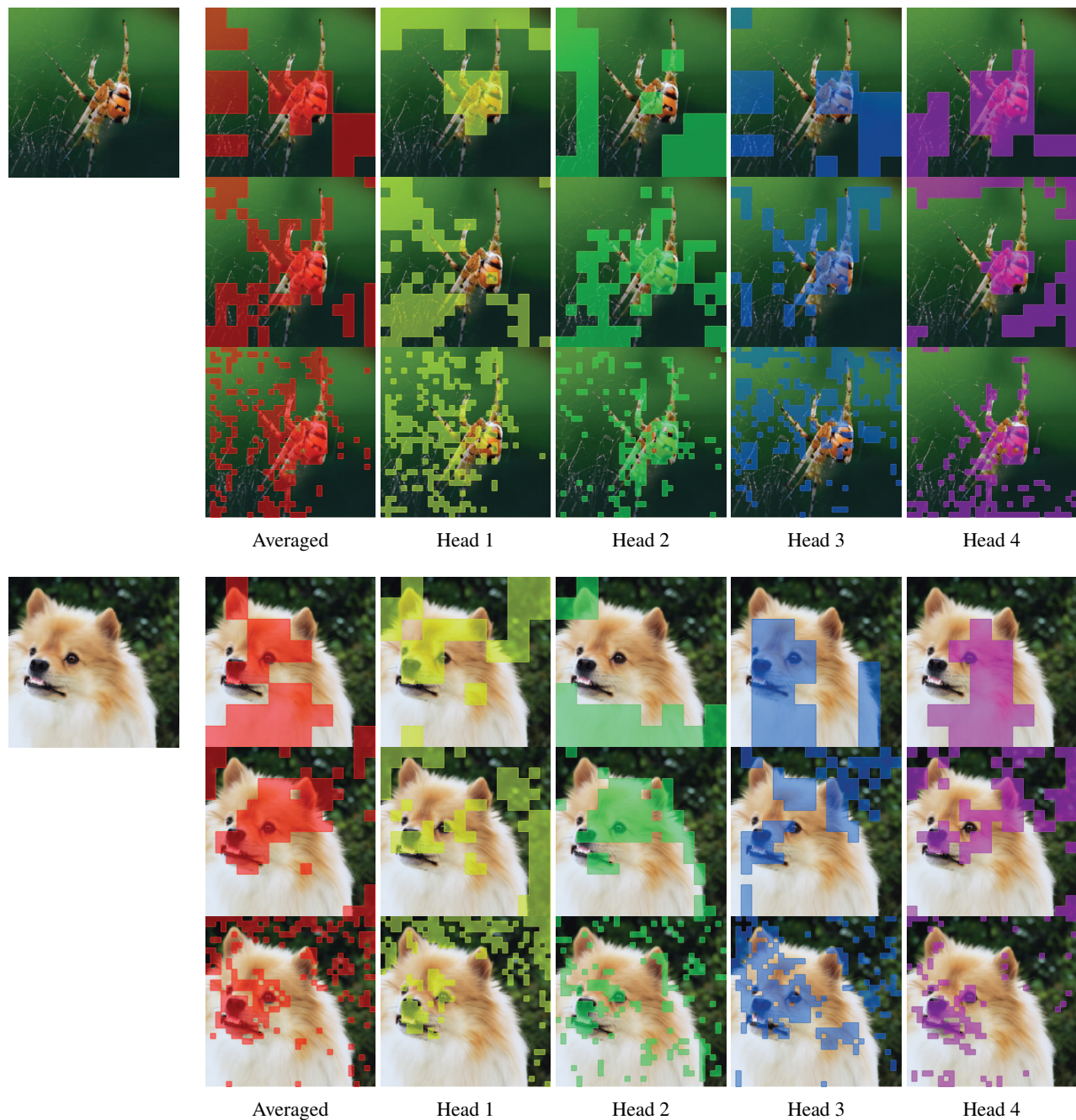


Figure 9: **Visualization of self-attention masks from different layers and heads.** Each row, top to bottom, corresponds to 8×8 , 16×16 and 32×32 self-attention layer, respectively.

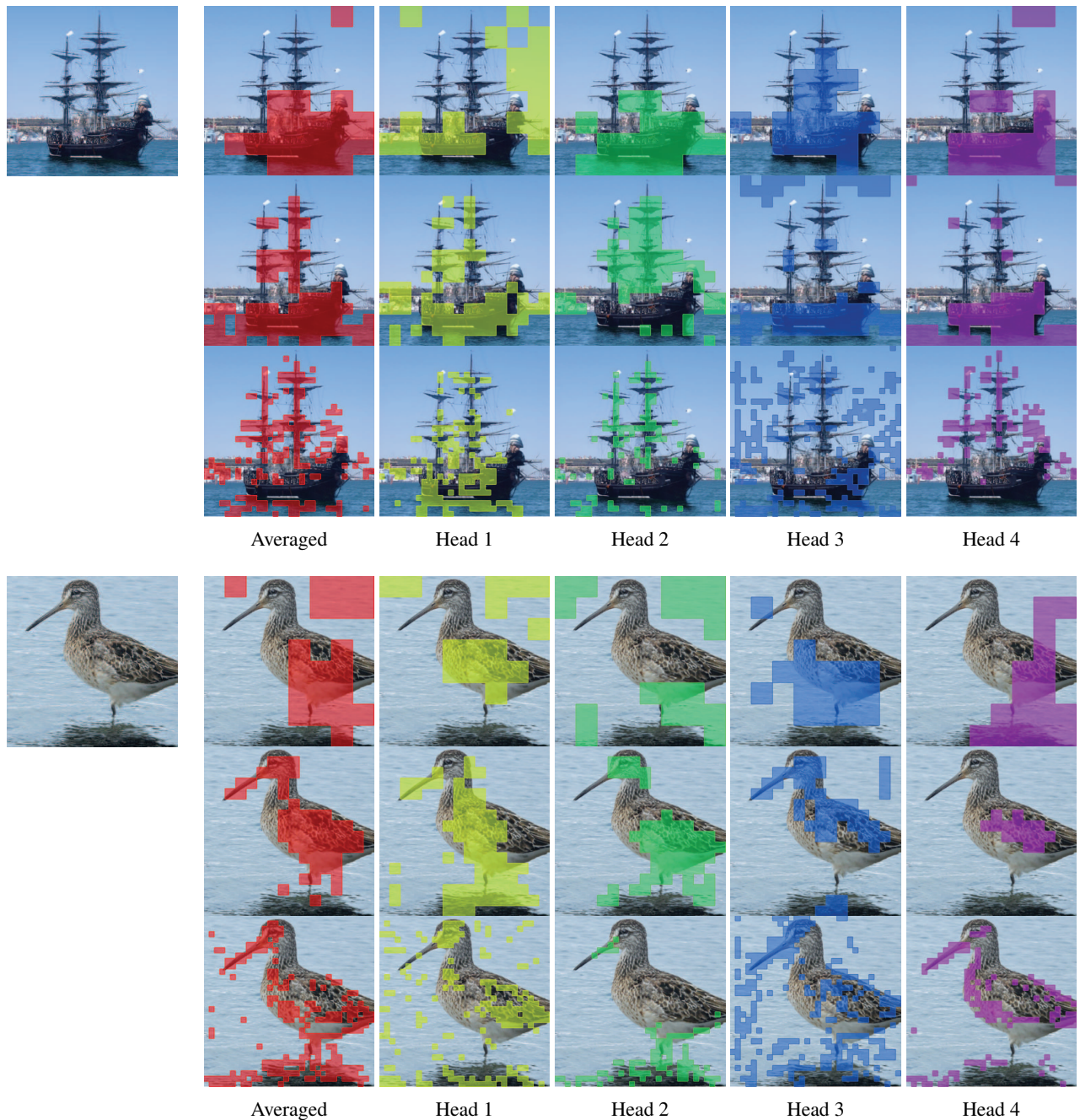


Figure 10: **Visualization of self-attention masks from different layers and heads.** Each row, top to bottom, corresponds to the 8×8 , 16×16 and 32×32 self-attention layer, respectively.

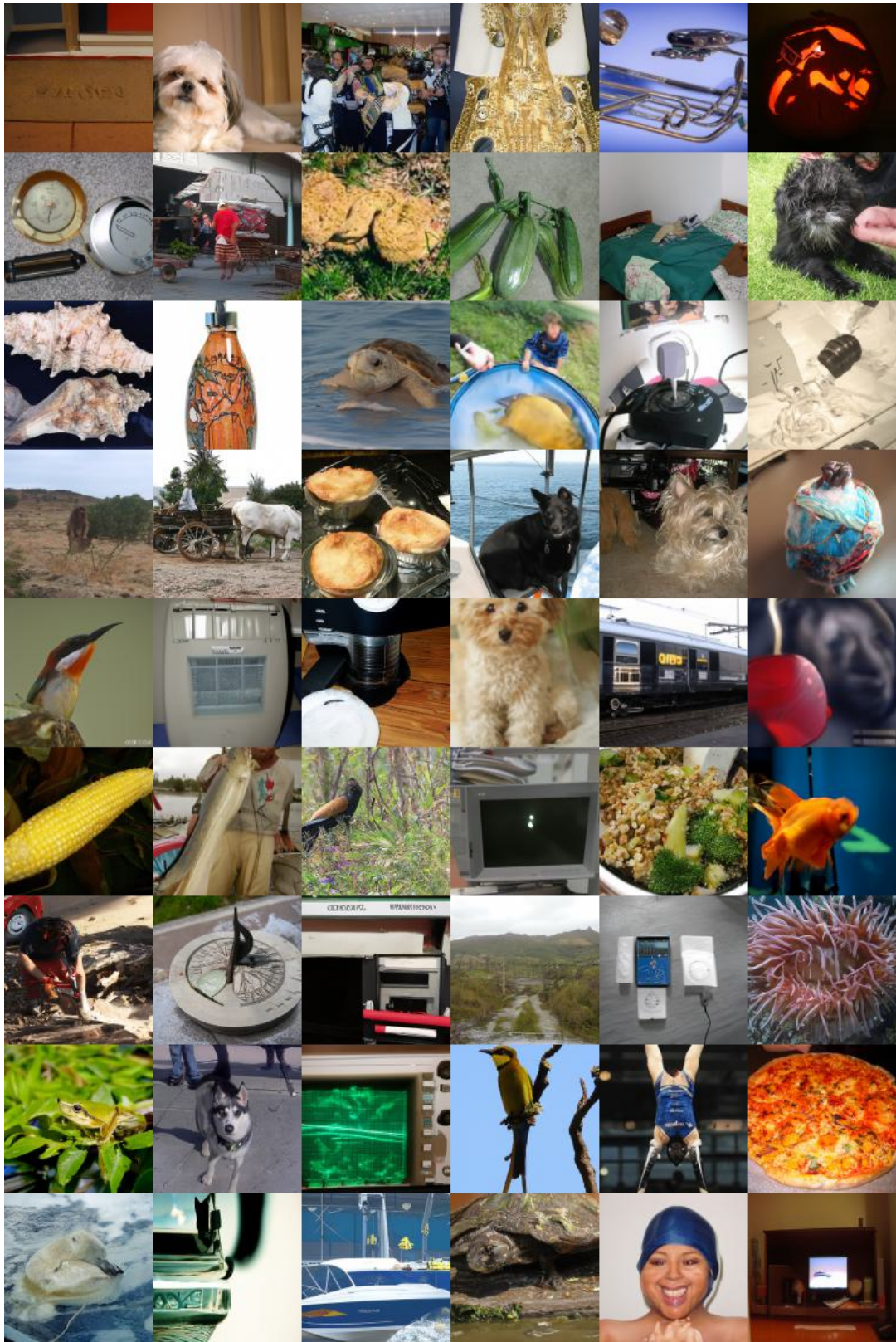


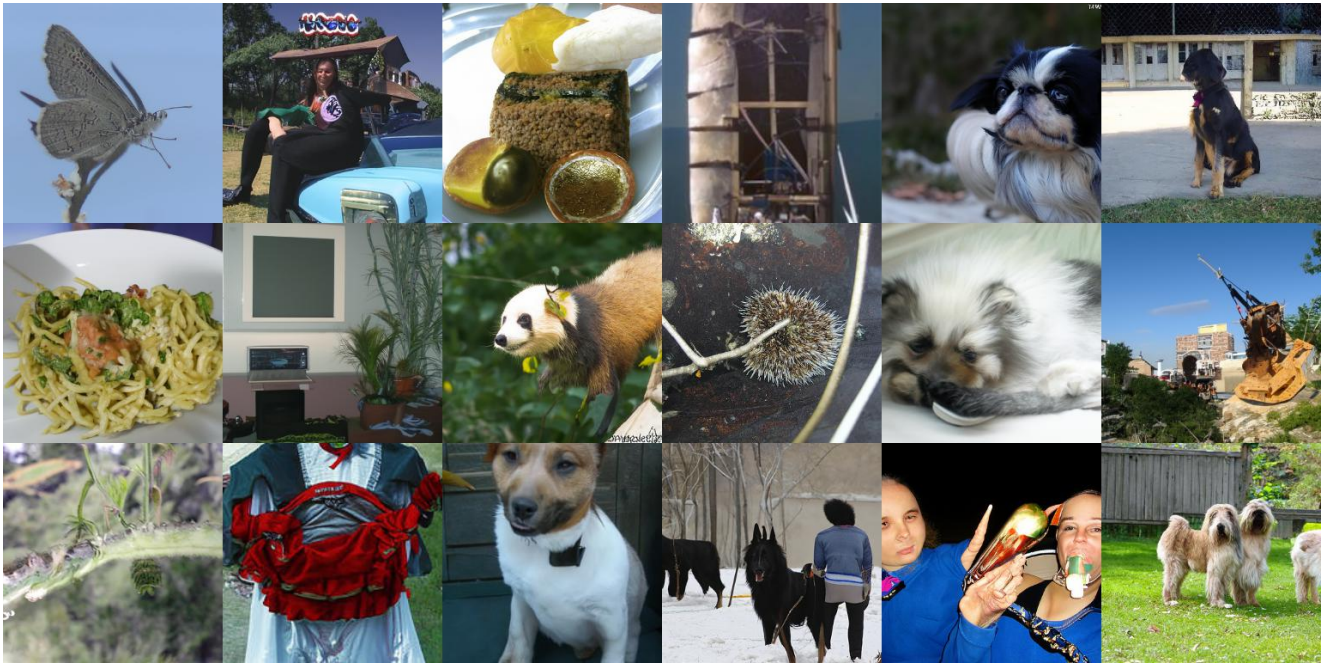
Figure 11: **Unselected samples from our method.** The results are sampled from ImageNet (Deng et al. 2009) 128×128 pretrained conditional model with self-attention and classifier guidance in combination.



Figure 12: **Unselected samples from our method.** The results are sampled from the pretrained weight of LSUN Cat (Yu et al. 2015) with self-attention guidance.



(a) Results from ADM (Dhariwal and Nichol 2021)



(b) Results from ADM (Dhariwal and Nichol 2021) with our method (SAG).

Figure 13: **Comparison of unselected samples between ADM (Dhariwal and Nichol 2021) and our method.** Both results are sampled from ImageNet (Deng et al. 2009) 256×256 pretrained unconditional model without classifier guidance. We use the same seed for both results and self-attention guidance is given to all the sampling steps.

Appendix C. Pseudo-code of Our Method.

We provide the pseudo-code of our method in Alg. 1, given a diffusion model $\text{Model}(\mathbf{x}_t)$ which outputs the predicted noise, variance, and attention map, and a masking function $\text{Mask}(A)$ described in the fourth section of the main paper. For Gaussian blur operation, we use transforms of torchvision module in PyTorch (Paszke et al. 2019).

Algorithm 1: Pseudo-code of self-attention guided sampling.

Input: guidance scale s

```

 $\mathbf{x}_T \sim \mathcal{N}(0, \mathbf{I})$ 
for  $t$  in  $T, T-1, \dots, 1$  do
   $\epsilon, \Sigma, A \leftarrow \text{Model}(\mathbf{x}_t)$ 
   $M \leftarrow \text{Mask}(A)$ 
   $\tilde{\mathbf{x}}_0 \leftarrow (\mathbf{x}_t - \sqrt{1 - \bar{\alpha}_t}\epsilon) / \sqrt{\bar{\alpha}_t}$ 
   $\tilde{\mathbf{x}}_0 \leftarrow \text{Gaussian-blur}(\tilde{\mathbf{x}}_0)$ 
   $\tilde{\mathbf{x}}_t \leftarrow \sqrt{\bar{\alpha}_t}\tilde{\mathbf{x}}_0 + \sqrt{1 - \bar{\alpha}_t}\epsilon$ 
   $\tilde{\mathbf{x}}_t \leftarrow (1 - M) \odot \mathbf{x}_t + M \odot \tilde{\mathbf{x}}_t$ 
   $\epsilon' \leftarrow \text{Model}(\tilde{\mathbf{x}}_t)$ 
   $\tilde{\epsilon} \leftarrow \epsilon' + (1 + s) \times (\epsilon - \epsilon')$ 
   $\mathbf{x}_{t-1} \sim \mathcal{N}(\frac{1}{\sqrt{\bar{\alpha}_t}}(\mathbf{x}_t - \frac{1 - \bar{\alpha}_t}{\sqrt{1 - \bar{\alpha}_t}}\tilde{\epsilon}), \Sigma)$ 
end for
return  $\mathbf{x}_0$ 

```

Appendix D. Limitations and Future Works

Our method has some points that need further research. First, it needs double feedforward steps to get the directions. This problem is the same issue classifier-free guidance (Ho and Salimans 2021) is facing, therefore needs to be alleviated in the future. Next, although we can simply use the pretrained models in this paper, modifying the training phase may help. For example, training with blur as in (Ho et al. 2022) may help the guidance to be more stable. Besides, our guidance method may fit well in diffusion models where the patches are embedded as tokens (Gu et al. 2022; Rombach et al. 2022). This will be an interesting subject to conduct further research on.